Journal of Applied Geophysics 111 (2014) 228–233

Contents lists available at ScienceDirect

Journal of Applied Geophysics

journal homepage: www.elsevier.com/locate/jappgeo

Seismic waveforms and velocity model heterogeneity: Towards a full-waveform microseismic location algorithm

D.A. Angus [a,*], A. Aljaafari [b], P. Usher [c], J.P. Verdon [c]

[a] Centre for Integrated Petroleum Engineering & Geoscience, University of Leeds, UK
[b] School of Earth & Environment, University of Leeds, UK
[c] Department of Earth Sciences, University of Bristol, UK

ARTICLE INFO

Article history:
Received 18 March 2014
Accepted 16 October 2014
Available online 25 October 2014

Keywords:
Full waveform
Location error
Microseismic
Ray theory

ABSTRACT

Seismic forward modeling is an integral component of microseismic location algorithms, yet there is generally no one correct approach, but rather a range of acceptable approaches that can be used. Since seismic signals are band limited, the length scale of heterogeneities can significantly influence the seismic wavefronts and waveforms. This can be especially important for borehole microseismic monitoring, where subsurface heterogeneity can be strong and/or vary on length scales equivalent to or less than the dominant source wavelength. In this paper, we show that ray-based approaches are not ubiquitously suitable for all borehole microseismic applications. For unconventional reservoir settings, ray-based algorithms may not be suitably accurate for advanced microseismic imaging. Here we focus on exploring the feasibility of using one-way wave equations as forward propagators for full waveform event location techniques. As a feasibility study, we implement an acoustic wide-angle wave equation and use a velocity model interpolation approach to explore the computational efficiency and accuracy of the solution. We compare the results with an exact solution to evaluate travel-time and amplitude errors. The results show that accurate travel-times can be predicted to within 2 ms of the true solution for modest velocity model interpolation. However, for accurate amplitude prediction or for higher dominant source frequencies, a larger number of velocity model interpolations is required.

1. Introduction

Microseismic monitoring is being applied increasingly in the hydrocarbon industry and this is because it provides a means of remotely monitoring the state of stress (i.e. failure) within the subsurface. Microseismic technology enables monitoring hydraulic fracture programs in unconventional reservoirs, assessment of fault reactivation and hydrocarbon leakage in conventional reservoirs, as well as characterization of the subsurface rock mass (e.g., frequency dependent seismic anisotropy). Although there has been significant development of advanced microseismic attributes (commonly referred to as 'beyond the dots in the box' by Eisner et al., 2010a), the location of microseismic events (the 'dots') represents the most fundamental measurement in microseismic monitoring (e.g., Eisner et al., 2010b).

Ray based solutions, such as eikonal solvers, are very attractive since they provide computationally fast solutions. If first-order effects of material averaging (or wavefront smoothing) can be modeled by a gradually varying medium and the wave path lengths are not too great, then basic ray methods should be applicable (e.g., Cerveny, 2001). However, ray based approaches are approximate solutions and do not accurately model wave phenomena when velocity heterogeneity varies on length scales on the order of or less than the dominant seismic wavelength (e.g., Angus, 2014; Cerveny, 2001). For instance, if strong multiple scattering or wide-angle diffraction is important, where seismic energy is scattered away from the direct ray path yet in the forward direction within the Fresnel zone, a numerical solution of the full wave equation is necessary (e.g., Carcione et al., 2002; Thomson, 1999). Full waveform approaches, such as finite-difference solvers, yield substantially more accurate solutions, but at the expense of slower computation times (e.g., Thomson, 1999). These full waveform solutions will yield very accurate solutions but, more often than not, may not be practical for microseismic processing. Thus, selecting an appropriate method involves weighing the advantages and disadvantages of all acceptable approaches in terms of accuracy requirements and computational limitations.

Usher et al. (2013) showed that microseismic waveforms are sensitive to velocity model and microseismic source frequency (this is fundamental to the physics wave propagation of bandlimited signals, i.e., frequency dependence of wave propagation). This dependence on velocity model and source frequency as well as unavoidable uncertainty in true velocity model will impact on the accuracy of microseismic event locations and hence reliability of any geometrical interpretation (Thornton, 2013). For instance, Thornton (2013) compared microseismic

* Corresponding author.
E-mail address: d.angus@leeds.ac.uk (D.A. Angus).

http://dx.doi.org/10.1016/j.jappgeo.2014.10.013
0926-9851/

travel-time predictions between an acoustic eikonal solver and a finite-difference solver, and observed noticeable mismatch between the two solutions. The results from Thornton (2013) are consistent with Usher et al. (2013) in that wave propagation is sensitive to velocity model heterogeneity, and that certain ray based approaches, being limited to smoothly varying velocity models, may not be universally suitable in all unconventional hydrocarbon settings. Ray based approaches neglect frequency-dependent effects and non-geometrical arrivals (e.g., head waves), and are generally only suitable for smooth velocity models (i.e., when heterogeneity length scales are greater than the dominant seismic wavelength).

In this paper, we explore the feasibility of using the wide-angle one-way wave equation as a forward propagator (i.e., Green's function) for microseismic event location. The wide-angle one-way wave equation is capable of modeling the waveform evolution along the underlying wavefront, where frequency dependent effects and non-geometrical arrivals can be predicted. We focus on borehole microseismic monitoring geometry, where wave propagation is predominantly sub-horizontal. In such circumstances, the influence of non-geometrical arrives due to horizontal layering as well as other wave phenomena due to velocity heterogeneity on lengths scales on the order of or less than the dominant seismic wavelength will be significant. For surface microseismic monitoring, the influence of vertical velocity variation is less problematic and so ray-based methods should be appropriate.

2. Theory

2.1. The influence of Green's function on event location error

To highlight the impact of velocity model and bandlimited wave propagation on microseismic waveforms and hence on event location uncertainty, we evaluate the influence of velocity model heterogeneity on event location using a ray-based location algorithm. Specifically, we use an eikonal solver to generate a look-up table for P- and S-wave travel-times through three depth-dependent 2D velocity models, thereby providing more realistic estimates of location error. A total of nine synthetic datasets are generated (Usher et al., 2013) by varying the velocity model and event dominant source frequency: three velocity models (3 layer surface seismic, 13 layer VSP and 34 layer sonic velocity models) and three geometrically equivalent microseismic events but with different dominant source frequencies (40 Hz, 150 Hz and 300 Hz). To generate the full waveform synthetics, we use the full waveform E3D code (Larsen and Harris, 1993). E3D is a staggered grid, fourth-order accurate in space and second-order accurate in time finite-difference algorithm (e.g., Virieux, 1984, 1986) for isotropic two-dimensional (2D) and three-dimensional (3D) viscoelastic media. The specific eikonal solver used was developed as part of the Madagascar package (Sethian, 1996; Sethian and Popovici, 1999). The eikonal solver is used to generate a look-up table of travel-times from each point in a discretized velocity model to each receiver. The optimum event location and uncertainty are evaluated using the neighborhood algorithm of Sambridge (1999a,b). The root-mean-square misfit between observed travel-time from the full waveform synthetic seismograms and the predicted travel-time from the ray-base eikonal solver is the objective function that is minimized. Since the eikonal solver produces travel-times for discrete points in the subsurface and the neighborhood algorithm requires the computation of a continuously varying hyper-surface, we use the interpolation algorithm of (Akima, 1978) to compute travel-times for points between the discretized grid of the eikonal solver.

In Fig. 1, we compare the influence of velocity model on event location for a microseismic source with dominant frequency 300 Hz (the results for lower dominant frequencies are similar). In this comparison, finite-difference synthetic microseismic waveforms are generated for three velocity models (3 layer surface seismic model, VSP and sonic log). The travel-times of the P- and S-waves are picked manually for each waveform data set. Locations for each of these sets of picks were computed using an eikonal solver using each of the three velocity models, giving a total of 9 permutations (3 velocity models used to generate synthetic data and 3 velocity models used in the event location algorithm). The resulting event locations are listed in Table 1.

First we consider the cases where the velocity model used to generate the synthetic data and the velocity model used to locate the events are identical (light blue, medium gray and dark red dots in Fig. 1). These results indicate the accuracy of the location algorithm, as any mislocation will come either from errors in picking, or from limitations in the use of eikonal solvers to compute travel-times: for instance, eikonal solvers compute the first arrival travel-time, regardless of whether this arrival is the most energetic arrival. For this case the locations are to within ± 5 m in depth. The horizontal distances range between 10 m and 40 m away from the modeled source location and this is due to the effects of array geometry; we use a single vertical borehole in this case. Using one or more additional boreholes would improve the horizontal location misfit (e.g., Jones et al., 2014). Note that for the sonic log model (dark red dot in Fig. 1), the confidence ellipse is larger indicating that the eikonal solver is yielding less accurate results as expected given that the model heterogeneity is beyond the ray theory high-frequency assumption. Next, we consider the cases where one velocity model has been used to generate the full waveform synthetic data, but the locations are computed using a different, and therefore incorrect, velocity model. The estimated source depths range between 5 m and 30 m of the true source depth, whereas the estimated source lateral locations range between 10 is 90 m from the true source lateral location. This suggests there is an error due to using different velocity models on the order of 10 m. We should note that this error is very optimistic (i.e., best case scenario) and we would expect error in real data to be larger, and this is because the synthetic waveforms are clean from typical microseismic noise.

2.2. Beyond ray-based algorithms—wide-angle one-way wave equation

Ray based forward modeling algorithms are extremely pervasive throughout the hydrocarbon industry because they provide very efficient travel-time predictions for a range of problems, such as velocity model building (e.g., Jones, 2010) and event locations (e.g., Maxwell, 2014). However, ray theory is a high-frequency approximate solution to the wave equation (Cerveny, 2001) and care must be taken when applying ray-based approaches to unconventional environments. Implicit in ray theory is the assumption that the velocity model heterogeneity is smoothly varying with respect to the length scales of the seismic wave. For microseismic events, assuming dominant frequencies ranging between tens of Hz up to hundreds of Hz (e.g., Gibowicz and Kijko, 1994; Maxwell, 2014; Rentsch et al., 2007; Teanby et al., 2004; Trifu et al., 2000), the wavelength of microseismic waves can range on the order of 100 s of meters for low frequency events down to 10 s of meters or less for higher frequency sources. For moderate to high frequency events (e.g., between 100 and 500 Hz signals), vertical velocity heterogeneity can be significant enough such that the ray theory assumption of smoothly varying velocity breaks-down (Thornton, 2013). This is especially problematic for borehole arrays since the velocity heterogeneity varies across the sub-horizontally propagating wavefront (Fig. 1). However, vertical heterogeneity also impacts surface array imaging, such as degrading imaging aperture (e.g., Price, 2013).

The one-way wave equation (sometimes referred to as parabolic wave equation) has been used extensively in the hydrocarbon industry primarily as a forward propagator in seismic reflection migration (e.g., Claerbout, 1970) but more recently in many other applications, such as modeling shear-wave splitting as well as frequency dependent anisotropy (see Angus, 2014). The one-way wave equation is computationally more efficient than full waveform solutions (e.g., finite-difference method) and this is because it reduces the second-order partial differential wave equation into two first-order equations

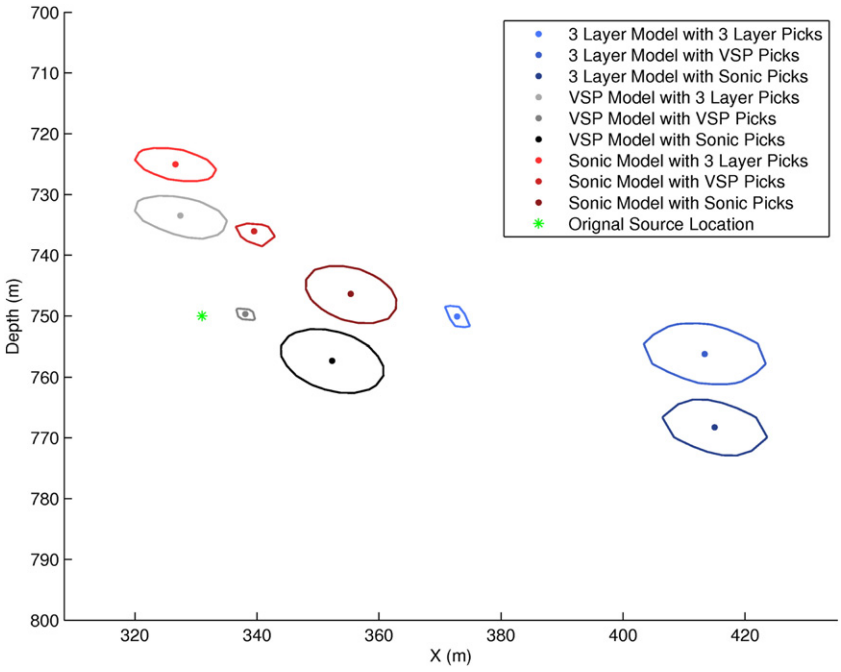

Fig. 1. Comparison of event locations using the eikonal solver with respective 90% confidence ellipses for a source with dominant source frequency of 300 Hz. The true source location is indicated by the green star. The blue values represent results where the synthetic waveforms were generated using the 3-layer velocity model, the gray/black using the VSP velocity model and the red using the sonic velocity model. The finite-difference algorithm E3D is used to generate the synthetic microseismic data and the travel times from the full-waveform finite-difference seismograms are picked manually. The eikonal solver uses the finite-difference full-waveform travel time picks to predict the event location.

(e.g., Angus, 2014; Fishmann and McCoy, 1984; Thomson, 1999). This reduction to first-order with respect to a preferred axis limits one-way wave equations to transmission problems, since backscatter is neglected, but allows a decrease in several orders of magnitude in computational effort (see Angus, 2014 for review of one-way wave equations). In this paper, we focus on the wide-angle one-way wave equation for 3-D acoustic media derived by Thomson (2005). The wide-angle acoustic equation is written as

$$\varphi(x_1+\varepsilon,x_\alpha,p_\alpha;\omega)=e^{[-i\omega P_1\varepsilon]}(1+Q\varepsilon)\varphi(x_1,x_\alpha,p_\alpha;\omega). \tag{1}$$

where ϕ is the acoustic wavefield, ε is the incremental extrapolation step length in the x_1 direction, x_α are the lateral coordinates (i.e., $\alpha = 2,3$), ω is frequency and p is slowness. The phase propagator coefficient P_1 is defined as

$$P_1(x_1,x_\alpha,p_\alpha)=\left[\frac{1}{V(x_1,x_\alpha)^2}-(p_\alpha)^2\right]^{1/2}, \tag{2}$$

Table 1
Event locations as computed using the eikonal solver. The 3 synthetic datasets were generated using the 3 velocity models. Travel-time picks for each dataset were then used to locate the event using the various velocity models (yielding 9 permutations). The relative location of the event is 330 m horizontally (lateral distance from the well) and 750 m in depth.

Velocity model for synthetics	Velocity model for location algorithm					
	Sonic		VSP		3 layer	
	Lateral (m)	Depth (m)	Lateral (m)	Depth (m)	Lateral (m)	Depth (m)
Sonic	355	746	352	757	415	768
VSP	340	736	338	750	413	756
3 layer	327	725	327	733	373	750

where $v(x_1,x_\alpha)$ is the 3D variable acoustic velocity. The transmission coefficient Q is the energy flux term

$$Q(x_1,x_\alpha,p_\alpha)=\frac{-\partial_1 P_1}{2P_1}, \tag{3}$$

that enables correctly modeling the true amplitude in the presence of strong velocity gradients.

Although Eq. (1) can be considered computationally efficient when compared to more complete full-waveform methods, such as finite-difference methods, it is still computationally cumbersome, especially for 3D media. One of the significant computational costs of this algorithm stems from the shuttling between the space and wave number domains (see Thomson, 2005); for many algorithms, this shuttling is done via very efficient fast Fourier transforms (FFTs). Improvements can be made by implementing theoretical approximations (Ferguson and Margrave, 2005) or by manipulating model parameterization (Gazdag and Sguazzero, 1984; Thomson, 2005).

To make the implementation of Eq. (1) computationally efficient, we make use of the velocity model interpolation concept introduced by Gazdag and Sguazzero (1984). Specifically, rather than having to compute an FFT at each grid point within the computational domain for each extrapolation step, an FFT is performed for an integer number of velocities. For each grid point, the wavefield is computed by linearly interpolating the wavefields from the nearest velocity values greater than and less than the individual grid velocity value. To do this, we introduce an automated linear interpolation scheme (Angus, 2014). In this approach, at each $x_1 + \varepsilon/2$ plane the acoustic velocity model is discretized into $i = (1, N)$ velocities

$$V_{min}(x_1+\varepsilon/2,x_\alpha)\le V_i\le V_{max}(x_1+\varepsilon/2,x_\alpha), \tag{4}$$

where V_{min} and V_{max} are the minimum and maximum acoustic velocities within the chosen velocity model, respectively. Next, the propagator P_1 and transmission coefficient Q are evaluated for each discrete

velocity V_i. Then N acoustic wavefields $\phi_i(x_1 + \varepsilon; \omega)$ are evaluated for each discrete velocity V_i using the wide-angle Eq. (1). Finally, for each lateral x_α grid point, the complete wavefield $\phi_i(x_1 + \varepsilon; x_\alpha, p_\alpha; \omega)$ is synthesized using the linear velocity wavefield interpolation (LVWI) scheme

$$\varphi(x_1+\varepsilon, x_\alpha, p_\alpha; \omega) = \eta_\alpha \varphi_i(x_1+\varepsilon;\omega) + (1-\eta_\alpha)\varphi_{i+1}(x_1+\varepsilon;\omega), \quad (5)$$

when $V_i \le V(x_1, x_\alpha) \le V_{i+1}$. The linear scaling factor is

$$\eta_\alpha = \left[1 - \frac{V(x_1, x_\alpha) - V_i}{\Delta V}\right] \quad (6)$$

and

$$\Delta V = \left[\frac{V_{min}(x_1+\varepsilon/2, x_\alpha) - V_{max}(x_1+\varepsilon/2, x_\alpha)}{N-1}\right]. \quad (7)$$

3. Results

To investigate the accuracy of implementing the automated LVWI scheme (Eq. (5)), we generate a suite of synthetic waveforms through the Horn River Basin velocity model of Maxwell (2009). Fig. 2 shows the 6-layer vertical P-wave velocity model for the shale-gas reservoir, where the targets for hydraulic stimulation are the Muskwa and Evie shales. To explore the accuracy of the velocity model interpolation approach, we compare the travel-time and amplitude predictions from Eq. (5) for $N = 2$ to $N = 7$ velocity model interpolations with the exact wide-angle equation (Eq. (1)). We compare the influence of source frequency for a range of six dominant source frequencies (50, 100, 125, 150, 250 and 500 Hz) and three source depths (upper shale at 2399 m, low velocity layer at 2510 m, and high velocity layer at 2490 m).

For all simulations, the wavefield is recorded along a vertical array (128 geophones spaced 6.3 m vertically) giving an aperture of approximately 800 m. Fig. 3 shows the wavefronts and waveforms for a seismic source located at 2399 m depth and having a dominant source frequency of 250 Hz. In this figure, it can be seen that as the number of velocity interpolants (N) increases the level of detail in the computed wavefield becomes sharper. Specifically, the computed waveforms and wavefield complexity due to the low and high velocity layers become more distinct and are much closer match to the exact solution as N increases to the total number of discrete velocities ($N = 7$).

The methodology used to compare the exact wide-angle wave equation predictions with the various velocity model interpolations uses cross correlation to evaluate the time lag between the primary arrivals. The computed time lag represents the estimated travel-time error. The amplitude error is calculated after first correcting for the time lag between the primary arrivals and then computing the maximum amplitude of the two time-corrected arrivals. The amplitude difference is expressed in terms of percentage difference from the exact wide-angle maximum amplitude.

Figs. 4–6 show the results of comparing the exact wide-angle solution with the LVWI for the 6 velocity model interpolations ($N = 2$ up to $N = 7$. In Fig. 4, we compare the amplitude difference (error) for each velocity model interpolation for the 6 frequencies. Increasing the velocity interpolants from $N = 2$ to $N = 7$ yields improved amplitude matches as expected. However, as the dominant source frequency increases so does the general amplitude error.

In Fig. 5, travel-time differences for each velocity model interpolation with respect to the exact wide-angle solution are shown for the 6 frequencies. Increasing the velocity interpolants from $N = 2$ to $N = 7$ yields improved travel-time matches as expected. For the travel-time predictions, the sensitivity to model interpolant and source frequency is less severe compared to the amplitude differences shown in Fig. 4. At $N = 2$, the travel-time error ranges between 5 ms and 10 ms, but for $N > 2$ these errors fall below 2 ms regardless of source frequency. It should be noted that the large travel-time errors computed for the low velocity model interpolant cases are an artifact of the conventional cross-correlation technique used (e.g., Whitecombe et al., 2010) related to the distorted waveforms (i.e., receivers 90 to 110 in Fig. 3) within the high/low velocity transition zone of the Mid-Devonian Carbonate layer and the Evie Shale layer.

In Fig. 6, we compare both the amplitude and travel-time differences for a 150 Hz dominant source frequency event but located at three

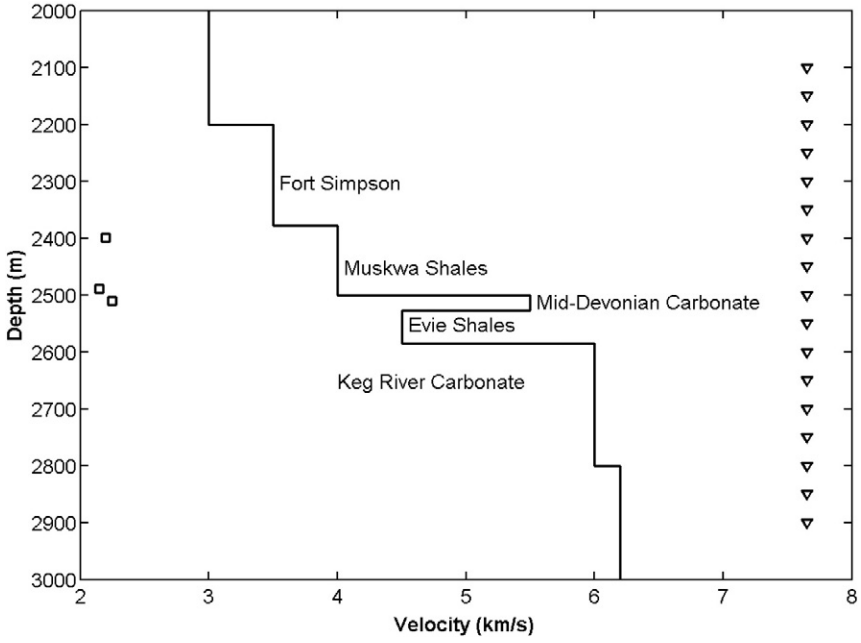

Fig. 2. P-wave velocity model of the Horn River Basin reservoir used in the wide-angle simulations. The square symbols on the left represent the relative depth of the three seismic sources. The inverted triangle symbols on the right show the relative depth extent of the vertical array consisting of 128 geophones. The lateral distance between source and geophone array is 250 m (not shown to scale in this figure).

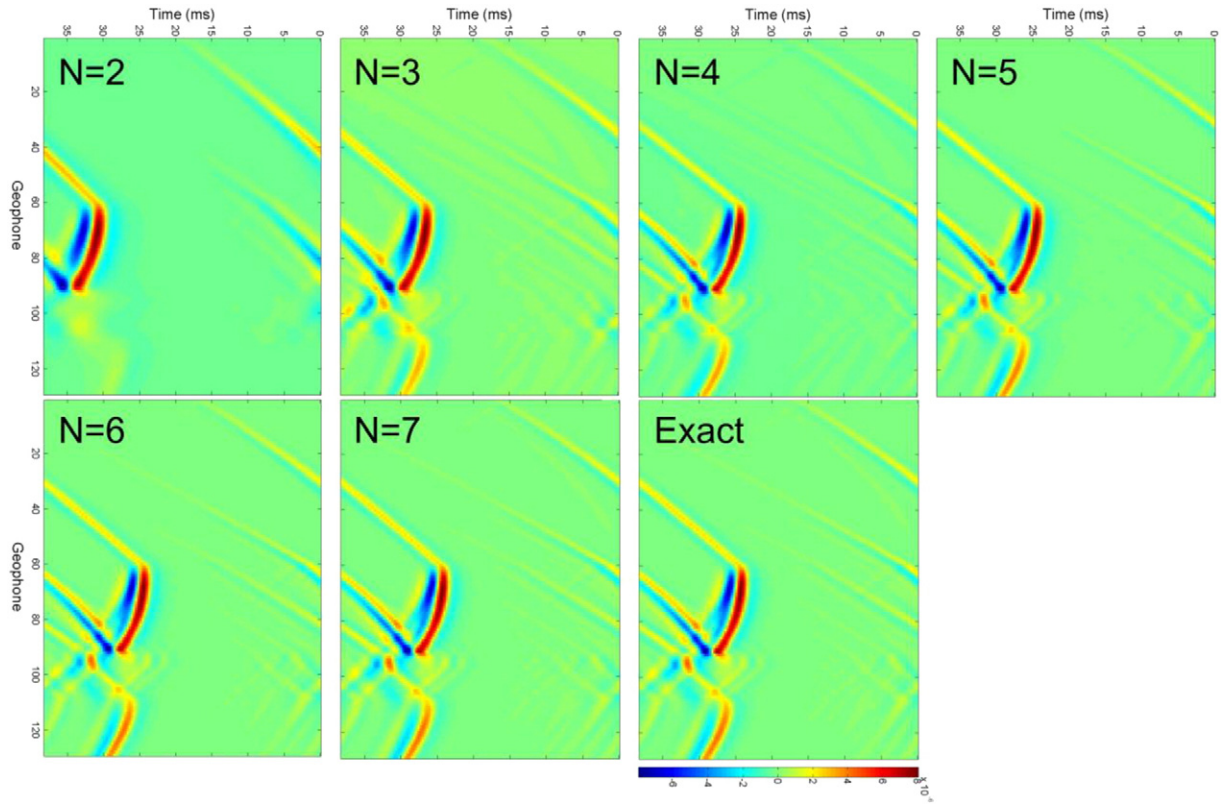

Fig. 3. Vertical snapshot of wavefield after propagating a total distance of 250 m horizontally for $N = 2, 3, 4, 5, 6$, and 7 number of velocity model interpolants, and the exact wide-angle solution. Since the time evolution of the wide-angle solution is computed in the frequency domain, the wavefield shows wrap-around in the time axis.

different depths; 2399 m within the Muskwa shale, 2490 within the Mid-Devonian carbonate, which acts as a high velocity layer, and 2510 within the Evie shale which acts as a low velocity layer (or wave guide). For all depths, the general trend of improving amplitude and travel-time prediction with increasing velocity model interpolant can be seen. Furthermore, there appears to be no significant influence of velocity contrast above and below the seismic event. Assuming travel-time picking error of 2–3 ms (e.g. Humphries, 2009; Kocon and van der Baan, 2012; Qiao and Bancroft, 2010), the results from Figs. 4–6 suggest a suitable value for model interpolation would be $N = 3$ or $N = 4$. However, if accurate amplitude information is required (e.g., for seismic moment tensor inversion) then $N > 4$ would be necessary.

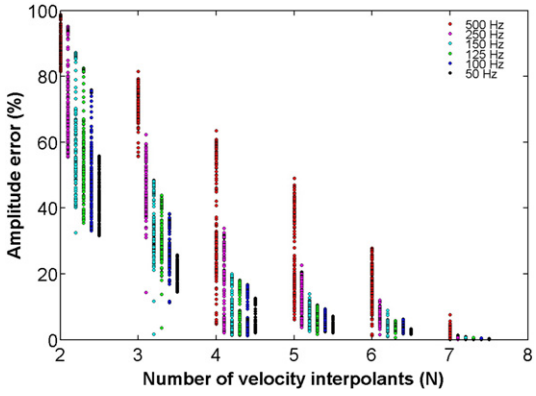

Fig. 4. Comparison of amplitude error in terms of % difference between the model interpolant (N) solution and the exact wide-angle solution for seismic event located at depth of 2399 m for all source frequencies.

4. Conclusions

We have shown that ray-based approaches are not necessarily always suitable for all microseismic applications. For instance, eikonal solvers compute very effectively the first arrival travel-time, regardless of whether this arrival has any energy observable above the noise. Furthermore, ray based approaches assume any velocity influence on travel-time is localized along the infinitely thin ray path and hence neglect velocity averaging that bandlimited seismic waves experience. Analysis of the influence of velocity model uncertainty and source frequency on location accuracy using an eikonal solver will be biased

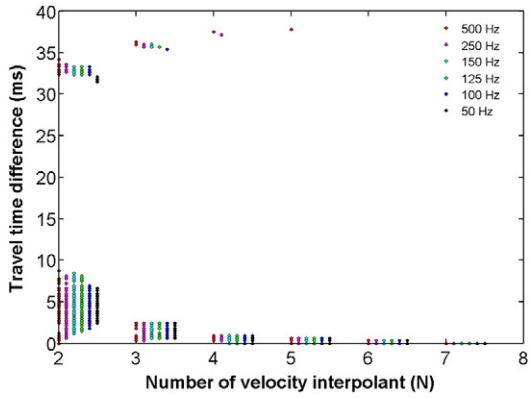

Fig. 5. Comparison of travel-time error (ms) between the model interpolant (N) solution and the exact wide-angle solution for seismic event located at depth of 2399 m for all source frequencies. The large travel-time errors (between 30 and 40 ms) are due to inaccurately modeled waveforms (i.e., receivers 90 to 110 in Fig. 3) within the high-to-low velocity transition of the Mid-Devonian Carbonate and Evie Shales (Fig. 2). The waveform distortion causes noticeable artifacts in the results of the conventional cross-correlation technique used.

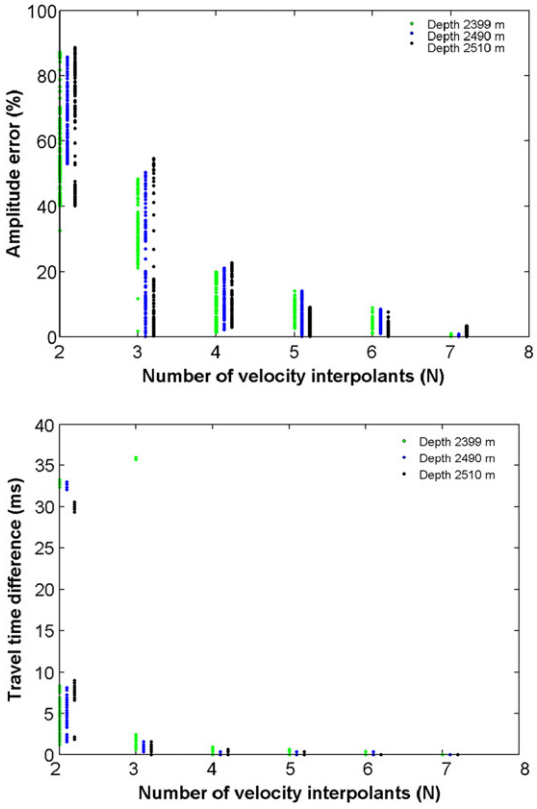

Fig. 6. Comparison of (top) amplitude error in terms of % difference and (bottom) travel-time error (ms) between the model interpolant (*N*) solution and the exact wide-angle solution for seismic event with dominant frequency of 150 Hz.

by the accuracy of the approximate forward propagator of the eikonal location algorithm. Thus error estimates from ray-based algorithms will not necessarily convey the true error. No amount of statistical sophistication can provide accurate error estimates if the forward model is not accurate enough. Thus, any mislocation will come not only from errors in travel-time picking and velocity model uncertainty, but also from limitations in the forward model (Green's function) used in the event location algorithm.

In this paper, we have studied the feasibility of using wide-angle one-way wave equations to compute travel-time and amplitude. Although it is difficult to improve velocity model uncertainty, we can certainly make improvements in the forward propagator in location algorithms. Here we examine one approach to achieve computational efficiency in the wide-angle wave equation and compare amplitude and travel-time prediction errors to the exact wide-angle solution. The results are promising considering that further computational and algorithm efficiencies can be made. Although these results are applied to acoustic media, the results have implications for wide-angle one-way wave equations for 3D elastic, anisotropic media.

Acknowledgments

The authors would like to acknowledge the sponsors of the ITF FRACGAS consortium (Chevron, EBN, ExxonMobil, Marathon Oil, Nexen, Noble Energy and Total) and phases 2 and 3 of the BUMPS consortium (BP, Chevron, CGG, Cuadrilla, ExxonMobil, Maersk Oil, Microseismic, PDO, Pinnacle, Rio Tinto, Schlumberger, Tesla, Total and Wintershall).

References

Akima, H., 1978. A method of bivariate interpolation and smooth surface fitting for irregularly distributed data points. ACM Trans. Math. Softw. 4, 148–159.
Angus, D.A., 2014. The one-way wave equation: a full waveform tool for modeling seismic body wave phenomena. Surv. Geophys. 35 (2), 359–393.
Carcione, J.S., Herman, G.C., ten Kroode, A.P.E., 2002. Y2K review article: seismic modeling. Geophysics 67 (4), 1304–1325.
Cerveny, V., 2001. Seismic Ray Theory. Cambridge University Press, Cambridge.
Claerbout, J., 1970. Coarse grid calculations of wave in inhomogeneous media with application to delineation of complicated seismic structure. Geophysics 35 (3), 407–418.
Eisner, L., Williams-Stroud, S., Hill, A., Duncan, P., Thornton, M., 2010a. Beyond the dots in the box: microseismicity-constrained fracture models for reservoir simulation. Lead. Edge 29, 326–333.
Eisner, L., Hulsey, B.J., Duncan, P., Jurick, D., Werner, H., Keller, W., 2010b. Comparison of surface and borehole locations of induced seismicity. Geophys. Prospect. 58, 809–820.
Ferguson, R., Margrave, G., 2005. Planned seismic imaging using explicit one-way operators. Geophysics 70, S101–S109.
Fishmann, L., McCoy, J., 1984. Derivation and application of extended parabolic wave theories. I. The factorized Helmholtz equation. J. Math. Phys. 25, 285–296.
Gazdag, J., Sguazzero, P., 1984. Migration of seismic data by phase shift plus interpolation. Geophysics 49 (2), 124–131.
Gibowicz, S.J., Kijko, A., 1994. An Introduction to Mining Seismology. Academic Press.
Humphries, M., 2009. Locating VSP diffracted arrivals using a microseismic approach. SEG Houston International Exposition and Annual Meeting, pp. 4184–4188.
Jones, I.F., 2010. An Introduction to: Velocity Model Building. EAGE Publications, Netherlands.
Jones, G.A., Kendall, J.-M., Bastow, I.D., Raymer, D.G., 2014. Locating microseismic events using borehole data. Geophys. Prospect. 62, 34–49.
Kocon, K., van der Baan, M., 2012. Quality assessment of microseismic event locations and traveltime picks using a multiplet analysis. Lead. Edge 31 (11), 1330–1346.
Larsen, S., Harris, D., 1993. Seismic Wave Propagation Through a low-Velocity Nuclear Rubble Zone. Lawrence Livermore National Laboratory.
Maxwell, S., 2009. Microseismic location uncertainty. CSEG Recorder, pp. 41–46, (April).
Maxwell, S., 2014. Microseismic imaging of hydraulic fracturing: Improved engineering of unconventional shale reservoirs. SEG Distinguished Instructor Series 17.
Price, D., 2013. The effect of anhydrite on the surface imaging of microseismic events(MSc dissertation) University of Leeds.
Qiao, B., Bancroft, J.C., 2010. Picking microseismic first arrival times by Kalman filter and wavelet transform. CREWES Research Report 22.
Rentsch, S., Buske, S., Luth, S., Shapiro, S.A., 2007. Fast location of seismicity: a migration-type approach with application to hydraulic-fracturing data. Geophysics 72 (1), S33–S40.
Sambridge, M., 1999a. Geophysical inversion with a neighbourhood algorithm-I: searching a parameter space. Geophys. J. Int. 138, 479–494.
Sambridge, M., 1999b. Geophysical inversion with a neighbourhood algorithm-II: appraising the ensemble. Geophys. J. Int. 138, 727–746.
Sethian, J., 1996. A fast marching level set method for monotonically advancing fronts. Proc. Natl. Acad. Sci. U. S. A. 93 (4), 1591–1595.
Sethian, J., Popovici, A., 1999. 3-D traveltime computation using the fast marching method. Geophysics 64 (2), 516–523.
Teanby, N., Kendall, J.-M., Jones, R.H., Barkved, O., 2004. Stress–induced temporal variations in seismic anisotropy observed in microseismic data. Geophys. J. Int. 156, 459–466.
Thomson, C.J., 1999. The 'gap' between seismic ray theory and 'full' wavefield extrapolation. Geophys. J. Int. 137, 364–380.
Thomson, C.J., 2005. Accuracy and efficiency considerations for wide-angle wavefield extrapolators and scattering operators. Geophys. J. Int. 163, 308–323.
Thornton, M., 2013. Velocity uncertainties in surface and downhole monitoring. EAGE 4th Passive Seismic Workshop PS08, Amsterdam, Netherlands.
Trifu, C.I., Angus, D.A., Shumila, V., 2000. A fast evaluation of the seismic moment tensor for induced seismicity. Bull. Seismol. Soc. Am. 90 (6), 1521–1527.
Usher, P.J., Angus, D.A., Verdon, J.P., 2013. Influence of a velocity model and source frequency on microseismic waveforms: some implications for microseismic locations. Geophys. Prospect. 61, 334–345.
Virieux, J., 1984. SH wave propagation in heterogeneous media, velocity-stress finite difference method. Geophysics 49, 1259–1266.
Virieux, J., 1986. P-SV wave propagation in heterogeneous media, velocity-stress finite difference method. Geophysics 51, 889–901.
Whitecombe, D.N., Paramo, P., Philip, N., Toomey, A., Redshaw, T., Linn, S., 2010. The correlated leakage method—it's application to better quality timing shifts on 4D data. 72nd EAGE meeting, Barcelona, Spain B037 (Extended Abstracts).